Ground-Penetrating Radar Imaging of Near-Surface Deformation along the Songino Active Fault in the Vicinity of Ulaanbaatar, Mongolia

Maksim Bano, Nyambayar Tsend-Ayush, Antoine Schlupp, Ulziibat Munkhuu

applied sciences

MDPI

Article

Ground-Penetrating Radar Imaging of Near-Surface Deformation along the Songino Active Fault in the Vicinity of Ulaanbaatar, Mongolia

Maksim Bano [1,*], Nyambayar Tsend-Ayush [1,2], Antoine Schlupp [1] and Ulziibat Munkhuu [2]

[1] EOST/CNRS, ITES UMR 7063, Université de Strasbourg, F-6700 Strasbourg, France; tsnyamka@gmail.com (N.T.-A.); antoine.schlupp@unistra.fr (A.S.)
[2] Institute of Astronomy and Geophysics, Academy of Sciences, Ulaanbaatar 13343, Mongolia; ulzibat@iag.ac.mn
* Correspondence: maksim.bano@unistra.fr; Tel.: +33-3-68850080

Abstract: The seismic activity observed in the vicinity of Ulaanbaatar (UB) capital city has been increased since 2005. Several active faults have been identified in the UB area. Most of the Mongolian population is concentrated around UB (1.5 million), which is the main political and economic center of the country. Hence, the study of seismic hazard is of first importance for the country. In this paper, we present the GPR results obtained on the Songino fault which is situated at 20 km west-southwest of UB at the northeast tip of Khustai fault. The combination of the morphotectonic, GPR and paleoseismological investigations brings essential information for seismic hazards assessments. The 2D GPR profiles are measured by using 250 and 500 MHz antennae and the topography using a differential GPS. An appropriate processing of the GPR data, including the topographic migration, allows us to bring out indirect characteristics of these faults. The objective is to identify near-surface geometry and coseismic deformation along the mapped fault. The 250 MHz GPR images of the Songino fault show the evolution of the sub-surface deformation mode induced by the arched geometry of the Songino fault. We observe a clear compressive structure at its NW section, strike slip at its central section and extensive structure in its SE part.

Keywords: GPR; active faults; Songino; Ulaanbaatar; deformation; Mongolia

Citation: Bano, M.; Tsend-Ayush, N.; Schlupp, A.; Munkhuu, U. Ground-Penetrating Radar Imaging of Near-Surface Deformation along the Songino Active Fault in the Vicinity of Ulaanbaatar, Mongolia. *Appl. Sci.* **2021**, *11*, 8242. https://doi.org/10.3390/app11178242

Academic Editor: Adriano Ribolini

Received: 22 June 2021
Accepted: 31 August 2021
Published: 6 September 2021

1. Introduction

During the 20th century, Mongolia was one of the most seismically active intra-continental areas in the world with four large earthquakes (above M 8) along its active faults in the western part of the country (Munkhuu et al., 2010 [1]; Schlupp et al., 2012 [2]). Despite that the seismic activity observed around Ulaanbaatar (UB), the capital of Mongolia (where about half of the population lives), is relatively low compared to the activity observed in Western Mongolia (Munkhuu et al., 2010 [1]), the study of seismic hazard and the estimation of the probability of future large and potentially destructive earthquakes are of first importance for UB and the country.

The observation of an increase of the seismic activity near UB since 2005 and the discovery of a new active fault, Emeelt, at about 10 km west of UB (Schlupp et al., 2012 [2]; Adiya, 2016 [3]) focused the attention in the area (Figure 1). The aim is to identify another unknown active structure and to characterize its activity. However, in the region, the geomorphology of the faults has been smoothed out due to erosion processes and a low slip rate (most likely less than 1 mm per year, Munkhuu et al., 2010 [1]); thus, the exact location of the fault is hidden in a several meter strip. In such a context, the GPR method has been proven to provide good results to characterize faults by identifying offsets of radar reflections and deformation along the strike of the fault (Christie 2009 [4]; McClymont, et al., 2010 [5]; Pauselli, et al., 2010 [6]; Yalçiner, et al., 2012 [7]; Beauprêtre et al., 2012 [8]; Dujardin, et al.,

2014 [9]; Maurizio et al., 2015 [10]). In general, features such as sedimentary structures, lithological boundaries, fractures and/or faults are clearly visible with GPR (Rashed et al., 2003 [11]; Deparis et al., 2007 [12]; Dujardin, 2014 [13]), even when these features differ only by small changes in the nature, size, shape, orientation and packing of grains (Guillemoteau et al., 2012 [14]). Therefore, several GPR campaigns were conducted near UB in 2012, 2013 and 2017 using 250 and 500 MHz shielded antennas (see Figure 2 for the position of the profiles) associated with differential GPS in order to measure the topography. In this study, we present the preliminary results of 2D GPR measurements performed along the Songino fault. This work is part of the complex characterization studies of active faults around the city of UB, capital of Mongolia.

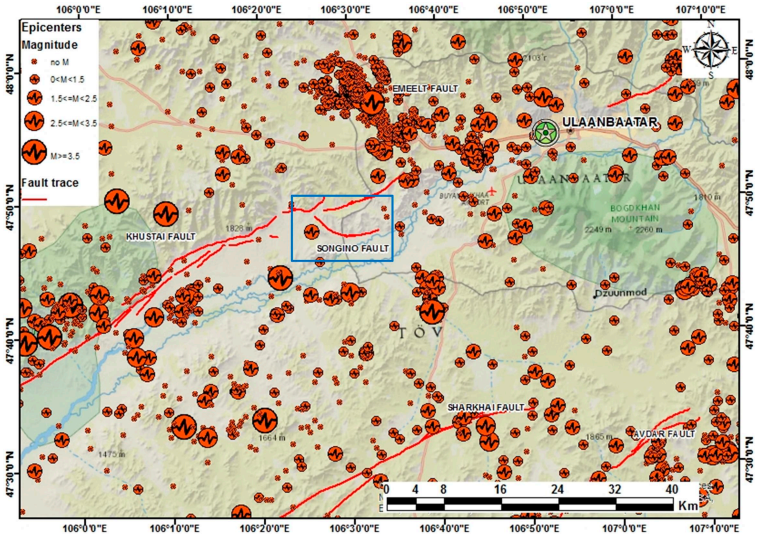

Figure 1. Seismicity map (orange symbols) around Ulaanbaatar city from 1994 to 2015 (NDC data, IAG, MAS). The green star indicates the UB city center. Red lines indicate the trace of main active faults. The Songino fault (blue rectangle) located between Emeelt and Khustai faults is about 20 km long and situated about 25 km SW of UB's western end.

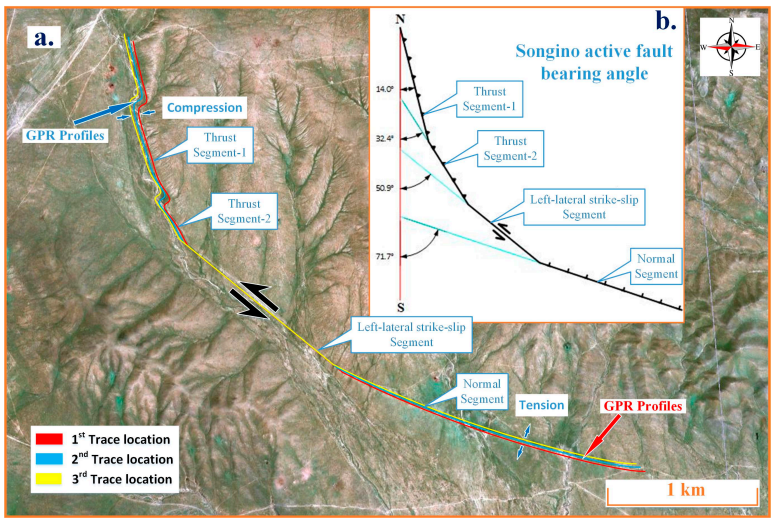

Figure 2. (**a**) Google Earth (2009) image showing the location of the Songino active fault. Red line indicates the 1st trace location, blue line represents 2nd trace location after the 1st seismic event, yellow one is the 3rd trace location after 2nd seismic event. (**b**) Modeling with time showing the variation in deformation process between NW (compressive), central (strike slip) and SE (extensive). The locations of GPR profiles discussed are indicated by blue (NW) and red (SE) arrows (modified from Tsend Ayaush, 2021 [15]).

2. Seismo-Tectonic Environment of UB Area

The Khustai fault's northeastern tip is located at 15 km west from Ulaanbaatar (Figure 1). This main fault of 80 km long may produce an M 7.5 earthquake, and it displays regular microseismicity with five events M 4+ and an M 5.4 since 1974 (Ferry et al., 2012 [16]). Exploratory trenches located along the central section of the active trace reflect the transtensional nature of the fault with mixed normal and left lateral strike slip, (Schlupp et al., 2012 [2]; Ferry et al., 2012 [16]).

The recently discovered Emeelt fault (swarm area in Figure 1) is located less than 10 km from the westernmost area of UB (Schlupp et al., 2012 [2]; Adiya, 2016 [3]). Its surface trace can be mapped over about 5 km and shows a right lateral strike slip with a vertical component. A paleo-river crossing the fault was mapped in detail by using a pseudo three-dimensional GPR profile (Dujardin et al., 2014 [9]; Dujardin, 2014 [13]). Previous studies show that the Emeelt fault could produce an earthquake with a magnitude of at least M 6.4 and up to M 6.7-7 (Schlupp et al., 2012 [2]; Dujardin, et al., 2014 [9]; Adiya, 2016 [3]). The Avdar and Sharkhai faults, located about 35 to 45 km south of the capital, are oriented between N040° E and N070° E at a length of about 45 km for each. They are left lateral strike slip faults that can be divided into several segments suggesting earthquakes magnitude between 6 and 7 (Al Ashkar, 2015 [17]).

The Songino Fault

The Songino Fault (see location in Figure 1) was discovered in 2012 by a geomorphological approach (Schlupp et al., 2012 [2]). Branched at the northeastern end of the Khustai active fault, it is about 20 km long and situated at 25 km southwest of UB. The geomorphology of the Songino fault is clearly visible on a high-resolution satellite image, with a smoothed but high scarp observed in the northwestern part of the fault (Figure 2). From northwest to southeast, the height of the Songino scarp gradually changes. While being quite high (about 20 m) at its northwestern end, it decreases towards the south before almost disappearing in some places in the middle. By continuing to the southeast, it gradually increases again up to about 0.5–1.5 m high. This is due to the curvature of the fault. The rather linear central part, oriented NW-SE with left lateral slip, induces at the northwestern end, nearly NS, a transpressional deformation and at the southeastern end, nearly EW, a transtensional deformation (Figure 2b).

No large earthquake has historically been reported on this fault; however, its structure gives indications of activity and a potential large seismic event (M 6.5) which could impact the city of UB.

3. GPR Investigations on Songino Fault

Several 2D GPR profiles were conducted across the morphological evidence of recent deformation at the SE transtensional section (see red arrow in Figure 2) in 2013 with 250 MHz and 500 MHz antennae (Tsend-Ayush et al., 2017 [18]; 2018 [19]) and at the NW transpressional section (see blue arrow in Figure 2) in August 2017 with seven close GPR profiles with 250 MHz shielded antenna. The aim was to image and describe, underneath the sedimentary sequence, its deformation induced by past earthquakes and describe the near surface geometry of the fault or deformation.

In this survey, we have used a Ramac GPR system, and the GPR profiles (see Figure 2 for the position of the profiles), perpendicular to Songino fault, have been acquired in Common Offset (CO) method. Traces are recorded every 2 cm for the 500 MHz antenna profiles and 5 cm for the 250 MHz antenna. A stack of 16 has been used to improve the signal to noise (S/N) ratio. Along with the GPR data lines, a differential GPS system has also been used in order to measure the topography. The processing of all GPR profiles has been performed with our own software written in Matlab (Dujardin et al., 2014 [9]; Dujardin, 2014 [13]). We used a common flow procedure including a constant shift to adjust the time zero, a dc filter to remove the low frequencies, a flat reflections filter to remove continuous flat reflections noise, a band-pass filter, a time varying gain function and finally

the topographic corrections. Band-pass filters are chosen to be 50–450 and 100–800 MHz for the 250 and 500 MHz antennae, respectively.

3.1. GPR Observation at Transpressional Part of the Fault (NW Part of Songino Fault)

GPR images still show the presence of sedimentary deposits, potentially datable and affected by deformations that could be related to previous earthquakes with clear offsets of radar reflections (Figure 3). The location chosen for GPR profiles (blue arrow in Figure 2) is where the fault affects deposits accumulated by a stream flowing from an eastern hill. The GPR image converted in depth (Figure 3) shows a clear thrust structure, with several compressive structures (red lines) in front of the scarp that has been smoothed since the last events. The black arrows indicate the movement direction of the deformation. The scarp height in this area is approximately 2 m and the uphill slope at east is about 4°. The deposits appear to be folded, but their complexity and the location of the GPR profile at the level of recent stream deposits with possible interbedded features should not be over-interpreted. The western part of the profile rises due to local erosion and is possibly related to the associated horizontal slip.

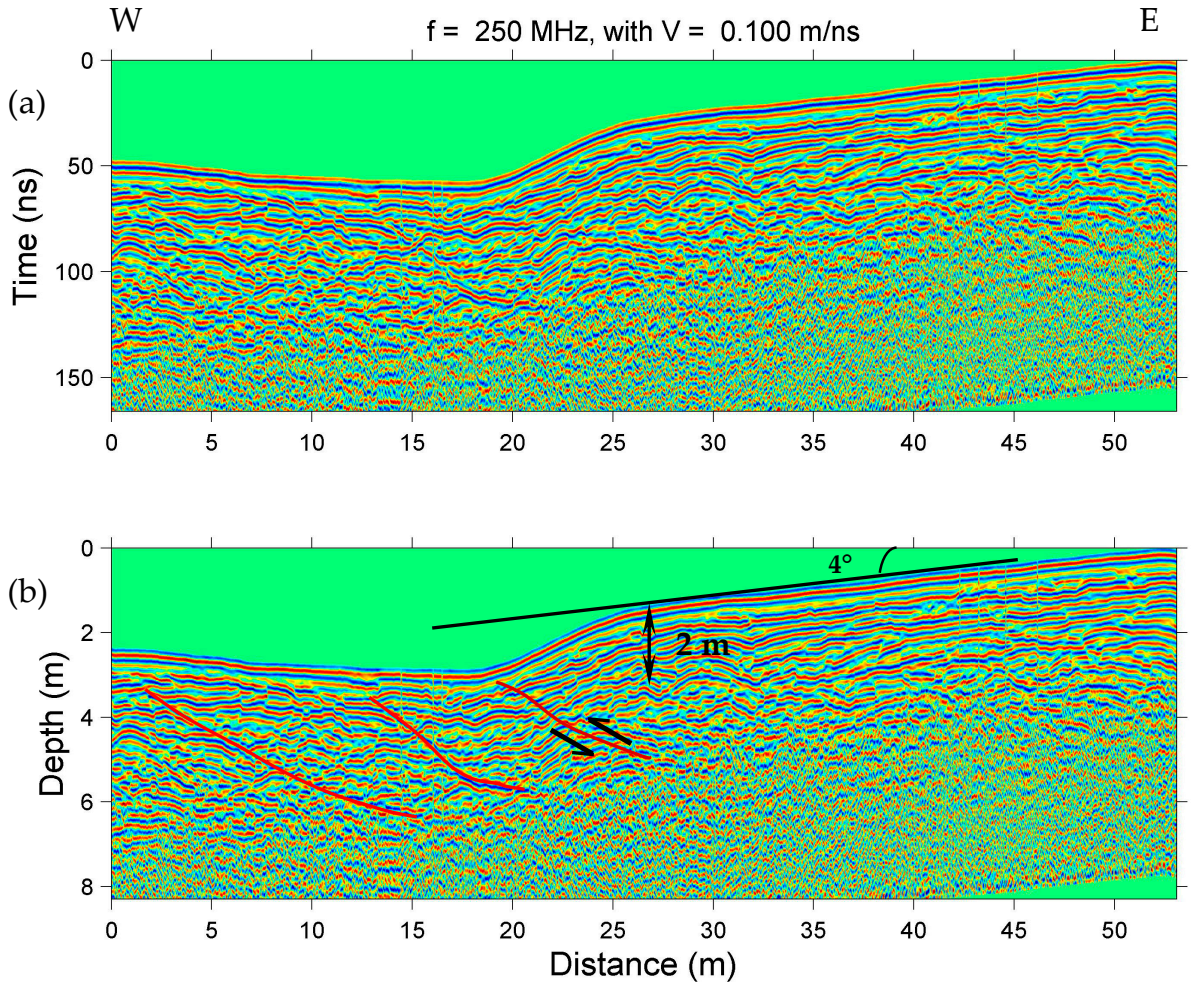

Figure 3. Result of GPR image of the profile 7 acquired in August 2017 with a 250 MHz antenna in the northwestern part of the Songino fault (blue arrow in Figure 2). (**a**) GPR image in time scale; the topographic correction is performed using a velocity of 0.1 m/ns. (**b**) Interpretation of the GPR image converted in depth, showing the thrust fault structure indicated by black arrows. The apparent scarp is about 2 m and the uphill slope is 4°. Red lines show compressive structures.

3.2. GPR Observation at Transtensionnal Part of the Fault (SE Part of Songino Fault)

The GPR profile with a 250 MHz antenna across the transtensional section of the fault (see red arrow in Figure 2) exhibits a strong reflection, which is offset (see white arrows). This vertical apparent displacement of about 1.3 m (Figure 4) probably does not correspond to the real vertical displacement as the fault is also associated with a strike-slip component. Indeed, when non-horizontal layers are affected by a pure strike-slip, a vertical shift (up or down) of these layers appears in a perpendicular section or trench. This process could account for a part of the vertical apparent displacement. In addition, the thickness of the sediment (composed of sand and silt) over this strong reflection is much greater uphill (left side of Figure 4) than downhill (on the right).It can be either due to a lateral shift (thicker sediments are moved laterally) or to deposits against a natural dam built by a vertical component on the fault (uphill, north) and lower deposits or even erosion (downhill, south). The GPR image shows a normal subsurface deformation that is enhanced by competent layer structure under the scarp (see white arrows). A change in GPR reflections is observed in the fault zone below the concave surface topography, indicating a filling zone with a different sedimentation and without visible stratification. The GPR reflections in this zone are less continuous compared to the reflections on both sides of the fault (uphill and downhill).

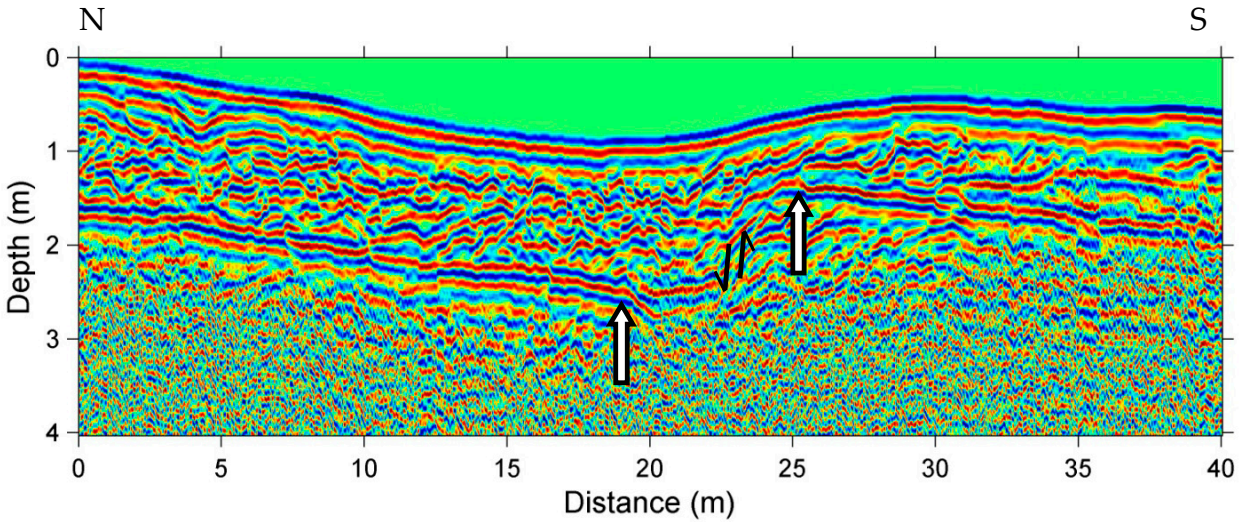

Figure 4. GPR image of the profile at the southeastern part of the Songino fault (transtensional fault zone, see red arrow of Figure 2) obtained with a 250 MHz antenna. The topographic correction is performed using a velocity of 0.1 m/ns. The GPR image shows a strong reflection (white arrows) that is affected and shifted by recent deformation. The black arrows indicate the apparent vertical movement along the fault zone.

Another GPR profile at about 150 m east of the previous one (red arrow in Figure 2) was conducted with a 250 MHz antenna in September 2012. The black arrow at around 48 m horizontally indicates the fault zone (Figure 5b).

On the left (north part) of the fault zone (black arrow at 48 m in Figure 5b), we observe reflections with a good continuity down to 1 m and a clear continuous reflection located between 20 and 40 m horizontally (white arrow of Figure 5b), whereas on the right of the fault zone (south part), the reflections are irregular and might correspond to the weathered bedrock. As in the case of Figure 4, the thickness of the sediment on the left of the scarp is more important uphill (left side in Figure 5) than downhill (on the right), showing a jump in the sedimentation process when crossing the fault zone. The height of the fault scarp in Figures 4 and 5 is around 0.5 m. On both GPR profiles, the uphill has been lowering, suggesting a counter-slope of the fault.

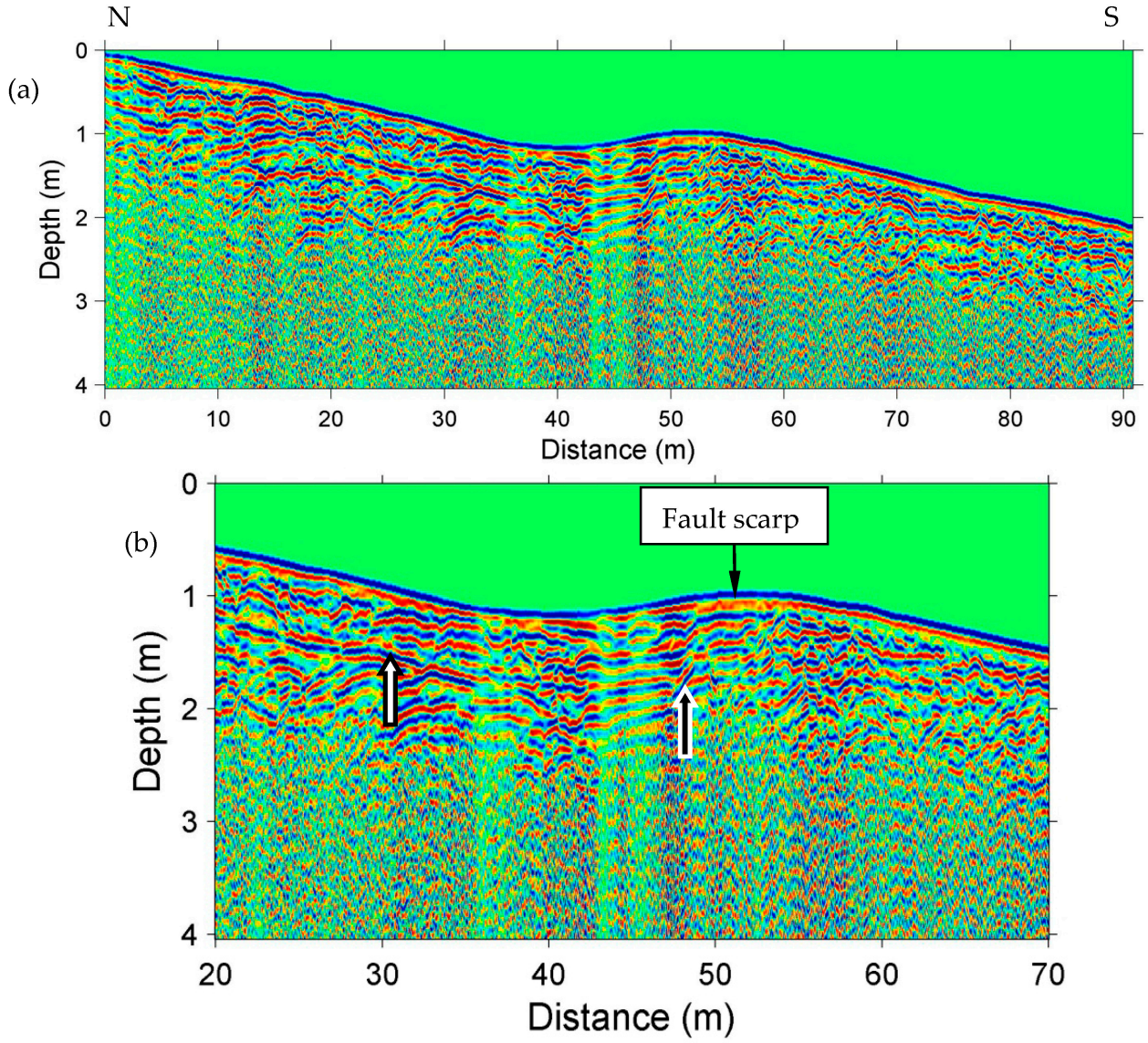

Figure 5. (**a**) GPR image of the profile at the southeastern part of the Songino fault (see red arrow of Figure 2 for the location) obtained with a 250 MHz antenna. The topographic corrections and depth conversion are performed using a velocity of 0.1 m/ns. (**b**) A zoom between 20 and 70 m horizontally is presented; black arrow indicates the fault zone. A change in GPR reflectivity is observed on both sides of the fault scarp at 52 m horizontally at the top of the smoothed fault scarp.

4. Discussion and Conclusions

The GPR profiles made it possible to image the underground structures at the two ends of the fault which are associated with opposite vertical deformations (compressive in NW, extensive in SE). The overall fault dip to the north-northeast, probably more vertical in its central section, inducing an extensive counter-slope scarp in the SE section with a recent accumulation of deposits. The 250 MHZ antenna appears to be the best adapted to the local context, with depth penetration close to the target for most of the paleo-seismological trenches of the order of 3 m.

The 250 MHz GPR images of the Songino fault show the evolution of the sub-surface deformation mode induced by the arched geometry of the Songino fault. We observe a clear compressive structure at its NW section, strike slip at its central section and extensive structure in its SE part with an apparent vertical displacement of around 1.2–1.3 m. This shows that it is necessary to make GPR measurement at various places along the fault to follow its behavior. As the fault is also associated with a strike-slip shift, a major component

at the central part decreasing toward the NW and SE, the observed vertical displacement in GPR profiles does not correspond to real offset.

These non-destructive observations allowed us to observe recent geological deposits, potentially datable, as well as sub-surface deformations induced by past earthquakes. This helps us to optimize the location of a paleo-seismological trench which will be presented in detail by Tsend-Ayush (2021 [15]), in preparation).

This study confirms that, after morphotectonic analysis, the GPR method contributes to the characterization of active faults, in particular near UB in Mongolia, in a context low slip rate where the geomorphologic features have been strongly smoothed due to erosion processes combined with a very long return period. The main result of this study is that it is possible to distinguish between active fault compression and tensile effects by combining the GPR imagery with the geomorphology of active faults.

Despite the very shallow penetration depth (up to 2–4.0 m with the 500 and 250 MHz antennae), the information obtained by the GPR profiles was very useful for better choosing the location of paleoseismological trench sites.

The next step of this study will be the paleoseismological investigations close to GPR profiles. These will be compared with our observations and GPR results before giving the final conclusions on this active fault and its relations with regional structures around UB city.

Author Contributions: Data curation, M.B., N.T.-A., A.S. and U.M.; investigation, N.T.-A.; methodology, M.B. and A.S.; validation, M.B. and A.S.; data acquisitions, N.T.-A., M.B., A.S.; field work, A.S., U.M. and M.B.; data processing, N.T.-A. and M.B.; writing—original draft preparation, M.B.; writing—review and editing, A.S. and M.B. All authors have read and agreed to the published version of the manuscript.

Funding: This research received no external funding.

Institutional Review Board Statement: Not applicable.

Informed Consent Statement: Not applicable.

Data Availability Statement: Data are available by the authors upon request.

Acknowledgments: The authors would like to thank Bayarsaikhan Enkhee for making the topographic measurements. Many thanks to Sarantsetseg Lkhagvasuren and the two students, Battsetseg Byambakhorol and Batdorj Nyamdavaa, who participated in the acquisition of the GPR data. We thank our colleague Matthieu Ferry for valuable discussions during the preliminary morphotectonic field survey. This work has been done in the frame of a long-term collaboration between France (University of Strasbourg—CNRS, EOST-IPGS-ITES) and Mongolia (Academy of Science of Mongolia, IAG).

Conflicts of Interest: The authors declare no conflict of interest. They have no known competing financial interests or personal relationships that could have appeared to influence the work reported in this paper.

References

1. Munkhuu, U.; Adiya, M.; Sebe, O.; Schlupp, A.; Usnikh, S.; Sodnomsambuu, D. The Emeelt active fault, revealed by the out-break of microseismicity, and its impact on the PSHA of Ulaanbaatar, Mongolia. Part II: Time and spatial behaviour of the regional seismicity, analysis. In Proceedings of the ESC 32nd General Assembly, Montpellier, France, 6–10 September 2010.
2. Schlupp, A.; Ferry, M.; Ulziibat, M.; Baatarsuren, G.; Munkhsaikhan, A.; Bano, M. Investigation of active faults near Ulaanbaataar. Implication for seismic hazard assessment. In Proceedings of the 9th General Assembly of Asian Seismological Commission, Extended Abstract, Ulaanbaatar, Mongolia, 17–20 September 2012; pp. 265–267.
3. Adiya, M. Seismic Activity Near Ulaanbaatar: Implication for Seismic Hazard Assessment. Ph.D. Thesis, University of Strasbourg, Strasbourg, France, 29 September 2016.
4. Christie, M.; Tsoflias, G.P.; Stockli, D.F.; Black, R. Assessing fault displacement and off-fault deformation in an exten-sional tectonic setting using 3-D ground-penetrating radar imaging. *J. Appl. Geophys.* **2009**, *68*, 9–16. [CrossRef]
5. McClymont, A.F.; Green, A.G.; Kaiser, A.; Horstmeyer, H.; Langridge, R. Shallow fault segmentation of the Alpine fault zone, New Zealand revealed from 2- and 3-D GPR surveying. *J. Appl. Geophys.* **2010**, *70*, 343–354. [CrossRef]

6. Pauselli, C.; Federico, C.; Frigeri, A.; Orosei, R.; Barchi, M.R.; Basile, G. Ground penetrating radar investigations to study active faults in the Norcia Basin (central Italy). *J. Appl. Geophys.* **2010**, *72*, 39–45. [CrossRef]
7. Yalçıner, C.Ç.; Altunel, E.; Bano, M.; Meghraoui, M.; Karabacak, V.; Akyüz, H.S. Application of GPR to normal faults in the Büyük Menderes Graben, western Turkey. *J. Geodyn.* **2013**, *65*, 218–227. [CrossRef]
8. Beauprêtre, S.; Garambois, S.; Manighetti, I.; Malavieille, J.; Sénéchal, G.; Chatton, M.; Davies, T.; Larroque, C.; Rousset, D.; Cotte, N.; et al. Finding the buried record of past earthquakes with GPR based palaeoseismology: A case study on the Hope fault, New Zealand. *Geophys. J. Int.* **2012**, *189*, 73–100. [CrossRef]
9. Dujardin, J.-R.; Bano, M.; Schlupp, A.; Ferry, M.; Munkhuu, U.; Tsend-Ayush, N.; Enkhee, B. GPR measurements to assess the Emeelt active fault's characteristics in a highly smooth topographic context, Mongolia. *Geophys. J. Int.* **2014**, *198*, 174–186. [CrossRef]
10. Maurizio, E.; Pauselli, C.; Romana, C.F.; Forte, E.; Volpe, R. Imaging of an active fault: Comparison between 3D GPR data and outcrops at the Castrovillari fault, Calabria, Italy. *Interpretation* **2015**, *3*, SY57–SY66. [CrossRef]
11. Rashed, M.; Kawamura, D.; Nemoto, H.; Miyata, T.; Nakagawa, K. Ground penetrating radar investigations across the Uemachi fault, Osaka, Japan. *J. Appl. Geophys.* **2003**, *53*, 63–75. [CrossRef]
12. Deparis, J.; Garambois, S.; Hantz, D. On the potential of Ground Penetrating Radar to help rock fall hazard assessment: A case study of a limestone slab, Gorges de la Bourne (French Alps). *Eng. Geol.* **2007**, *94*, 89–102. [CrossRef]
13. Dujardin, J.R. Imagerie Géoradar (GPR) en Milieu Hétérogène : Application aux Failles Actives en Mongolie et aux Dépôts Pyroclastiques du Tungurahua (Equateur). Ph.D. Thesis, University of Strasbourg, Strasbourg, France, 22 September 2014.
14. Guillemoteau, J.; Dujardin, J.-R.; Bano, M. Influence of grain size, shape and compaction on georadar waves: Examples of aeolian dunes. *Geophys. J. Int.* **2012**, *190*, 1455–1463. [CrossRef]
15. Tsend-Ayush, N. Characterization of Active Faults by2D and 3D Ground Penetrating Radar Imaging Technique and Interpretation of the Results. Ph.D. Thesis, University of Strasbourg, Strasbourg, France, 2021.
16. Ferry, M.; Schlupp, A.; Munkhuu, U.; Munschy, M.; Fleury, S. *Tectonic Morphology of the Hustai Fault (Northern Mon-Golia)*; EGU General Assembly: Vienna, Austria, 2012.
17. Al Ashkar, A. Tectonique active de la Région d'Oulan Bator, Mongolie: Analyse Morphotectonique et Paléosismologique. Ph.D. Thesis, University of Strasbourg, Strasbourg, France, 2015; 249p.
18. Tsend-Ayush, N.; Bano, M.; Schlupp, A. Songino active fault from GPR imaging and trench results, Ulaanbaatar, Mongolia. In Proceedings of the International Conference on Astronomy and Geophysics, Ulaanbaatar, Mongolia, 20–22 July 2017.
19. Tsend-Ayush, N.; Baño, M.; Schlupp, A.; Munkhuu, U.; Davaasambuu, B.; Byambakhorol, B.; Khuut, T. Studying active faults by combing GPR images with morphotectonic and trenching results. In Proceedings of the EAGE-HAGI 1st Asia Pacific Meeting on Near Surface Geoscience and Engineering, Yogyakarta, Indonesia, 9–13 April 2018; pp. 1–5. [CrossRef]